Article

Not peer-reviewed version

Design of a Novel Intraoperative Sensor for Load Balancing and Tracking during Total Knee Replacements

Samira Al-Nasser *, Siamak Noroozi, Adrian Harvey

Posted Date: 23 April 2024

doi: 10.20944/preprints202404.1464.v1

Keywords: joint force measuring; soft tissue balancing; intraoperative sensors; artificial intelligence; total knee replacement

 doi:10.20944/preprints202404.1464.v1

Article

Design of a Novel Intraoperative Sensor for Load Balancing and Tracking during Total Knee Replacements (TKR)

Samira Al-Nasser [1,*], Siamak Noroozi [1] and Adrian Harvey [2]

[1] Bournemouth University, Design and Engineering, Poole, England; snoroozi@bournemouth.ac.uk
[2] Royal Bournemouth Hospital, Bournemouth, England
* Correspondence: salnasser@bournemouth.ac.uk

Abstract: Intraoperative load sensors have been developed with the aim of balancing the soft tissue in the knee during Total Knee Replacements (TKRs). Literature has shown success in soft tissue balancing however, concerns regarding the accuracy of these sensors remain. For this reason, previous research has attempted to create robust sensors for intraoperative use. The design of the sensor in this research has aimed to address the concerns outlined in the literature to create a new and novel smart-sensor for soft-tissue balancing. This new intraoperative load sensor included design features to increase accuracy while artificial intelligence allowed for comprehensive sensing across the entirety of the sensor, providing unparalleled insight during the operation. Notably, the sensor was designed to withstand loads of at least 450 N, ensuring robust performance of the sensor. To optimize the design process while minimizing cost, Finite Element Analysis was employed. This approach ensured the design features fulfilled their function while maintaining structural integrity to withstand loads. Moreover, the novelty of using training data from simulated data will reduce the iterative process of the labor-intensive collection of training data for the artificial intelligence while reducing human error associated with it. Results from the evaluation demonstrated the ability of this design to successfully bridge the current gap in the market by fulfilling all essential design criteria established within the literature. This innovative smart-sensing tool will in turn enhance patient outcomes and alleviate financial burdens to patients and the healthcare systems by reducing the need for early revision surgeries associated with improper joint tension.

Keywords: joint force measuring; soft tissue balancing; intraoperative sensors; artificial intelligence; total knee replacement

1. Introduction

The soft tissue, namely ligaments, surrounding the knee are responsible for the passive stability of the joint [1,2]. The stability or lack thereof in the knee is a principal factor for success during a Total Knee Replacement (TKR) operation which is required when the cartilage in the joint is worn causing pain, discomfort, or functional problems. The tension created by the soft tissue surrounding the knee is responsible for the passive forces creating stability in the knee [3]. Intraoperative sensors aim to accurately measure tibiofemoral contact forces in real time throughout a range of motion (ROM) [4]. The need for such devices was apparent in a study by Batailler et al. where at least 60% of TKRs needed additional balancing procedures, where having a quantitively balanced knee provided higher patient satisfaction scores [5].

Functional improvements, like postoperative ROM and gait analysis, to the knee have also been observed when the surrounding soft tissue was balanced. For example, a 6-minute walking distance showed significant improvements when the knee was balanced intraoperatively with a sensor [6]. Ample research supported this idea where postoperative instability was reported as a major cause for early TKR revisions [7–9].

 doi:10.20944/preprints202404.1464.v1

However, some disagreement was present about the correlation between balanced knees and postoperative improvements. Livermore et al. reported no improved short-term patient-reported outcome measures (PROMs), radiological outcomes, or ROM when compared to conventional TKR techniques [10]. However, the accuracy of the sensor in ensuring the joint was balanced intraoperatively could be questioned.

Although still debated in literature the argument for the importance of having a well-balanced knee outweighs the research arguing the opposite in terms of quantity and impact. Additionally, the absence of a robust sensor for measuring the loads intraoperatively may be contributing to the arguments against load balancing.

Criteria for a Measuring Device

The new adaptable intraoperative, tibial sensors aim to quantify and track load and position data through a range of laxity testing and flex-extension cycles to give orthopedic surgeons the necessary haptic and numeric data that supports a decision regarding balancing the soft tissue and positioning the implant.

Without such sensors, surgeons are required to rely on bony landmarks to optimize the alignment between the tibial and femoral components which is suboptimal or less accurate at best. For intraoperative sensors to achieve proper results, according to Roth et al., the design of the device must adhere to the following criteria [11]:

- Must function in real time
- Must be interchangeable with the tibial base tray which is a part of the TKR implant system
- Must be able to identify the location of the center of pressure and the total magnitude of the applied force
- Must detect and interpolate the peak femorotibial contact point over the whole surface of the implant where the sensing area covers the whole surface including the edge of the sensor
- Must be able to identify the load and track its location in both the medial and lateral compartments simultaneously
- Must have repeatable outputs with low error margins for the force at different contact points
- Must be able to withstand up to 450 N force at the contact points to identify any imbalances in tension

Various companies and researchers have attempted to create intraoperative load sensors for TKRs, however one that fits all the criteria does not yet exist [12–26]. There were two commercially available sensors, VERASENSE by Orthosense and later bought by Stryker and eLibra by Zimmer Biomet. As of 2023, eLibra was no longer in use and there are plans for the removal of VERASENSE from the market. This leaves a gap in the market for an accurate tool for intraoperative use for TKRs. Both eLibra and VERASENSE were unable to satisfy all the criteria set by Roth et al. Moreover, independent knee joint sensors for measuring tibiofemoral joint forces have been designed since 1996 with new sensors being created as of 2023.

2. Design of a New Generation of Smart Adaptive Intraoperative Load Sensors

The new design of a knee transducer sensor for use intraoperatively relied on several key design criteria. The aim was to produce a robust tool for accurate measurement of contact force and its location in real time.

The key features include:

1. Being adaptable for use with other knee implants systems.
2. Interchangeable with the tibial spacer
3. Compatible with different implant systems
4. Variable curved surface to mimic natural knee and for congruency with femoral implant through the range of motion.
5. Reduced or minimal load sharing between compartments
6. Optimum total load transfer path through the 3 sensors in each compartment.
7. Adaptable and easy to use of adjustment tools to balance the initial soft tissue tension.

 doi:10.20944/preprints202404.1464.v1

8. Using spacer to increase the overall tension in the joint.

During intraoperative use, the sensor sits between the femur and the tibia and on top of the tibial tray to measure the loads in the knee seen in Figure 1. This design is adaptable to fit most knee implant systems on the market with little modification to the adjustment or balancing tensioner.

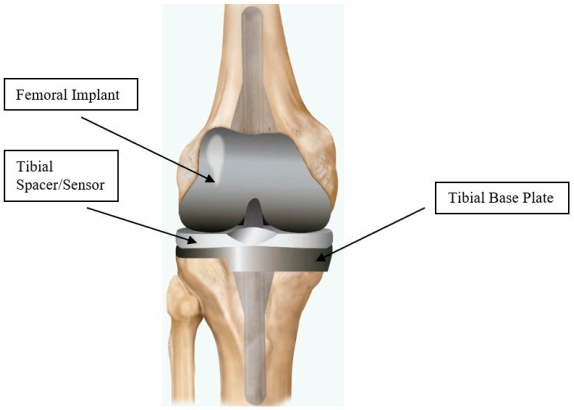

Figure 1. Placement of sensor in the knee in relation to knee replacement implant system.

These points were all considered during the physical design of the sensor. In addition, there are three more key design features also implemented. They included a) separate, but partially locked, medial and lateral compartments, b) the interchangeable ring mechanism to adjust the height to match the existing insert thickness., c) to minimize mechanical cross talk and eliminate load sharing new design transfers all the load through the 3 tabs holding the sensors to increase in accuracy (Figures 2 and 3).

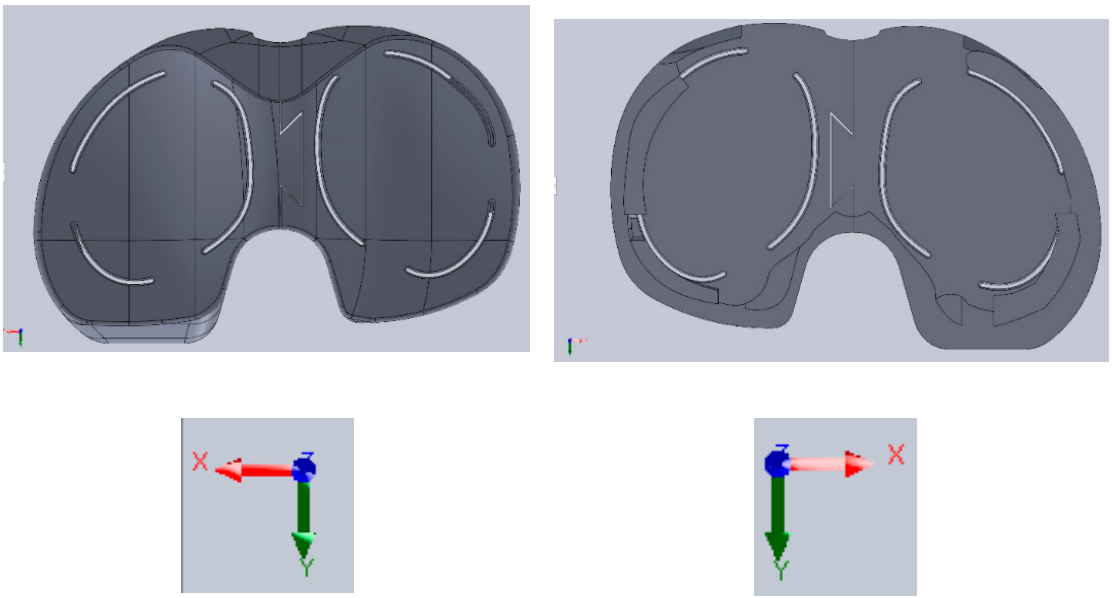

(**a**) (**b**)

Figure 2. Tibial sensor design **a)** Top view **b)** Bottom view.

 doi:10.20944/preprints202404.1464.v1

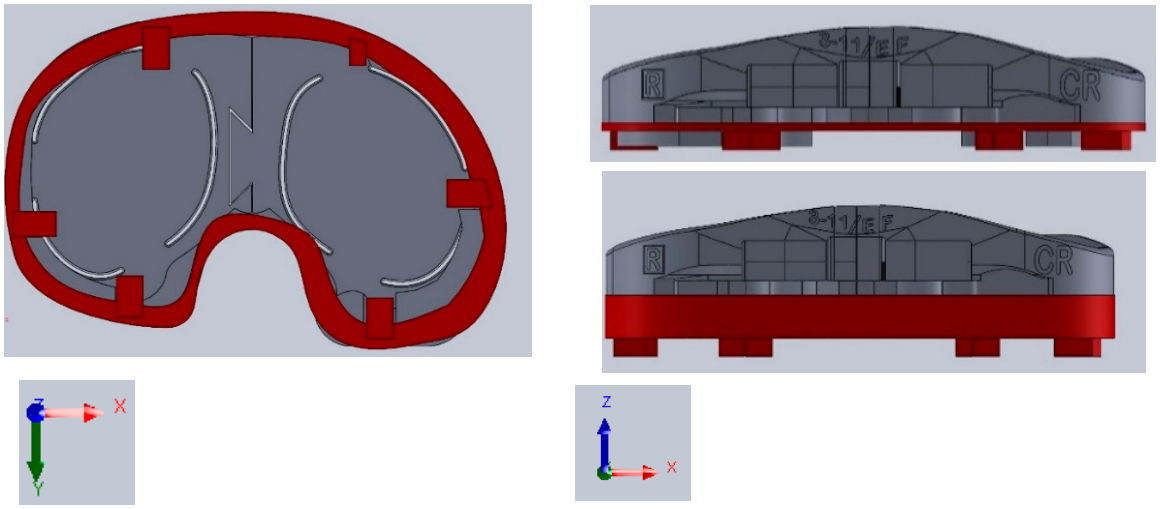

(**a**) (**b**)

Figure 3. Tibial sensor with ring attached for increasing joint tension **a)** 1 mm ring attached (bottom view) **b)** 1 mm vs 6 mm ring attached (front view) for increased thickness of sensor/increased tension.

The use of a dovetail, Figure 2, allowed movement in the Z-axis (vertical to the top of the tibia tray) but limited the separation or the lateral displacement of the two compartments in the X and Y-axis. This allowed for the load in one compartment to not be shared with the applied load in the other compartment. Moreover, the 3 slits on the top surface of each compartment were designed to transfer all the load into the tabs between where the 3 sensors were placed. This was to reduce mechanical crosstalk resulting in unique solution thus increasing the accuracy of the device by concentrating the load to appear on the tabs. Hence increasing the signal to noise ratio.

The height adjustment feature can be used to match the thickness of the implant insert, which were made in 1 mm increments as was standard for knee implants. The red in Figure 3 is the ring attached the sensor where the thicker rings will provide more tension in the joint.

3. Validation of Design Using Finite Element Analysis (FEA)

As a design feature it was important for the sensor to withstand a load of up to 450 N. Also, to ensure principal stresses line up with the tabs and their associated sensors and that there was limited load sharing between compartments. A validated FEA model was used to ensure that the design fulfilled these criteria.

The Ring and base were constrained in the same manner that would be attached to the ring, where there was a local contact interaction established between the dovetails (Figure 4). The locations of the strain gauges were added to the tabs with the size 1.8mmx1.0mm.

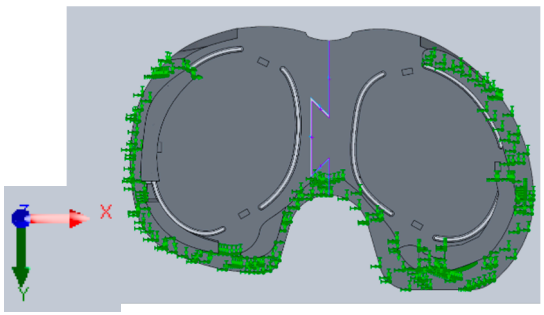

Figure 4. Fixtures and Connections

3.1. Convergence Study

 doi:10.20944/preprints202404.1464.v1

A detailed convergence study was performed to determine the coarseness/fineness for purpose of the mesh. A converged model offers the trade-off between accuracy and computational costs.

Each compartment was meshed independently, and both compartments used a blended-curvature mesh with tetrahedral elements (Table 1). For each compartment, a total of 7 different mesh densities were used and the effect on stress at key points were compared. Since this was the first prototype, an aluminum alloy was used. It was chosen since it was cost-effective, light weight, strong, and homogeneous and as stress is independent of the material properties the success of this sensor can be used to confirm the success of the same sensor in a different material.

Table 1. Mesh number with total number of elements for each compartment.

	Medial Compartment	Lateral Compartment
Mesh Number	**Total Number of Elements**	**Total Number of Elements**
1	4677	3721
2	16573	23445
3	69098	59211
4	98067	70736
5	111388	91865
6	143888	126407
7	182771	144160

A point force of 200 N was applied at the center of each compartment (Figure 5) and the average Von Mises stress over the tab area where the strain gauges are placed was recorded.

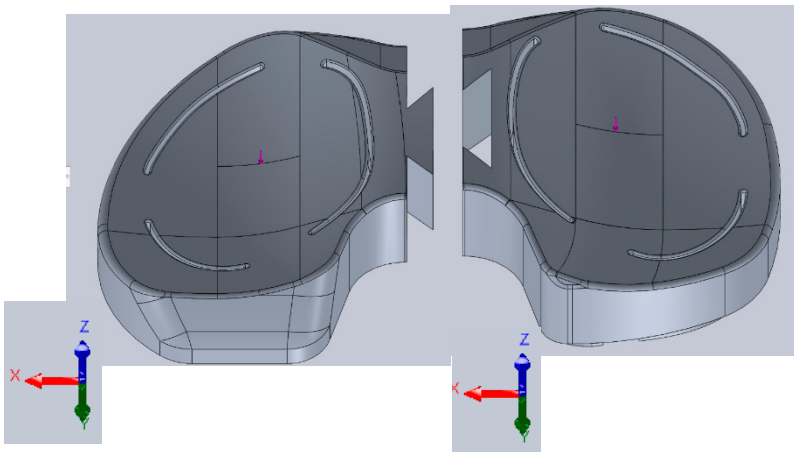

(**a**) (**b**)

Figure 5. Location of applied load (200 N) **a)** Medial load **b)** Lateral load.

The results of the medial compartment indicated that the Mesh 3 provided a sufficient mesh density to give repeatable and reliable stress results. Figure 6a shows the percent difference between stress results using Mesh 3 compared to Mesh 4, which was only 0.65%. However, the difference between Mesh 1 and Mesh 3 was 12.12% indicating stability in the results when Mesh 3 was used.

For the lateral compartment, Mesh 3 was of a sufficient size and density as shown (Figure 6b) where there was a percent difference of less than 1% between Mesh 3 and Mesh 4, 5, 6, and 7 while the percent difference between Mesh 1 and Mesh 3 was 4.09%.

Preprints.org (www.preprints.org) | NOT PEER-REVIEWED | Posted: 23 April 2024 doi:10.20944/preprints202404.1464.v1

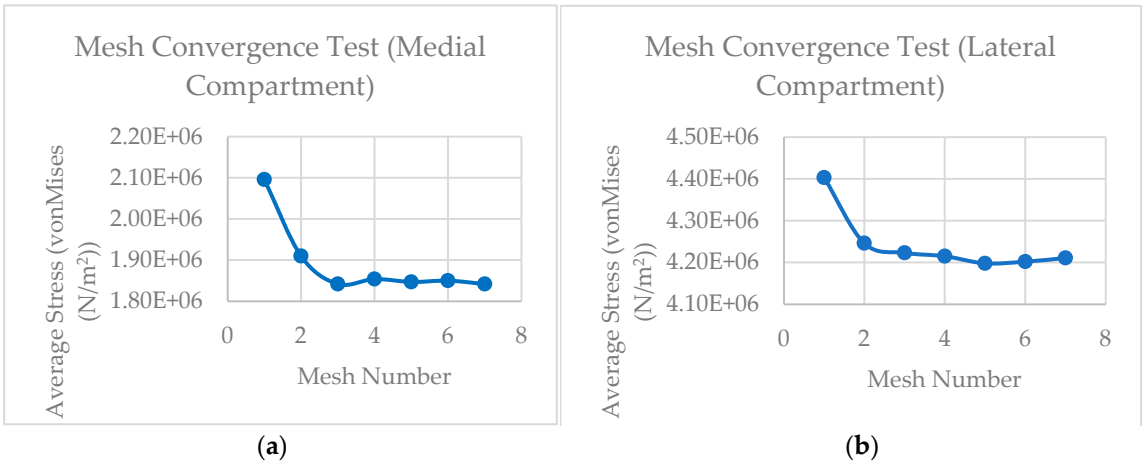

Figure 6. Mesh convergence **a)** Medial compartment **b)** Lateral compartment.

The final mesh used for subsequent FEA can be seen in Figure 7, where the total number of elements was 128,309.

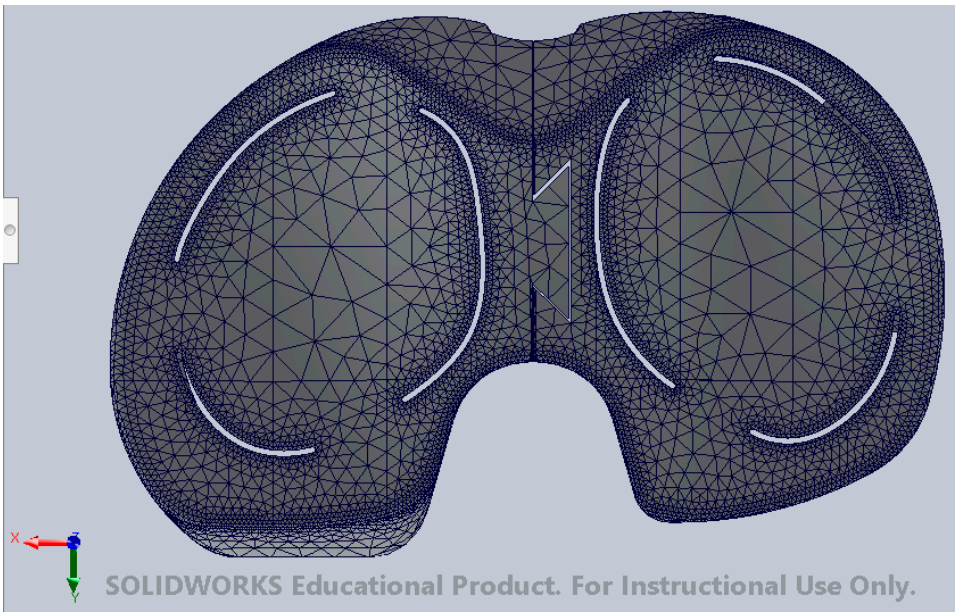

Figure 7. Final mesh

3.2. Defining an External Effects of Contact Effects of Different Point Load Definition

In theory, the slits ensured the force was transferred through the 3 tabs where the strain gauges were placed. This is to minimize load sharing and mechanical crosstalk. Therefore, the method of applying the point load should be independent of the stress at those tabs. It was decided to investigate the effect of different definitions of a point load. To accomplish this, five different external loads were applied to the same location on the surface of the sensor. The same mesh density and constraints were used in all cases. In each case the loads were applied to the medial compartment. To mimic the use of a ball bearing, two spherical areas (radius of 1mm and 2mm) were created on the surface of the tibial sensor FEA models, Figure 8.

 doi:10.20944/preprints202404.1464.v1

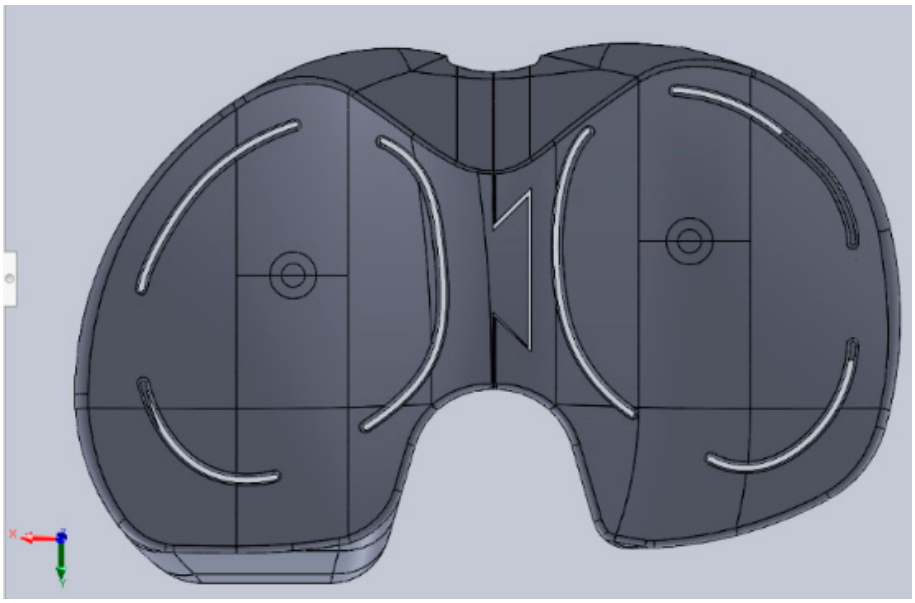

Figure 8. Location of applied load.

To apply 200 N as pressure, the surface areas were measured and divided by the 200 N force. In total, the pressures applied were 15.91 MPa for the 4mm diameter circle and 63.69 MPa for the 2 mm diameter circle. A list of the 5 different types of forces applied is detailed in Figure 9.

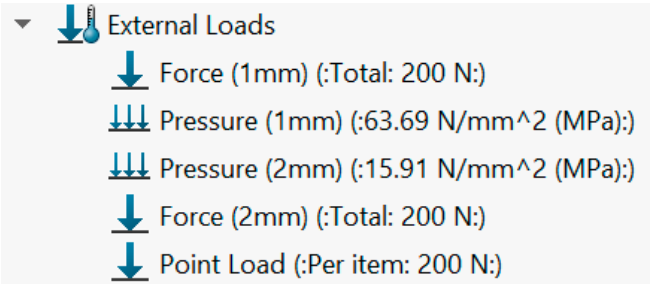

Figure 9. Types of loads applied

The result for all loading methods, Figure 9, were recorded and the average Von Mises stresses were calculated. The results, Figure 10, show that there was no significant difference in Von Mises stresses on the tabs or location of the strain gauges. This indicated the tabs were far enough from the applied load and load intensities were normalized or diffused by the time it reached all 3 tabs. This is quite significant in stress analysis as it ensures minimum distortion of the tabs during testing between the outputs. Therefore, for all the subsequent analyses and training data collections, a point load will be used to apply the loads.

Preprints.org (www.preprints.org) | NOT PEER-REVIEWED | Posted: 23 April 2024 doi:10.20944/preprints202404.1464.v1

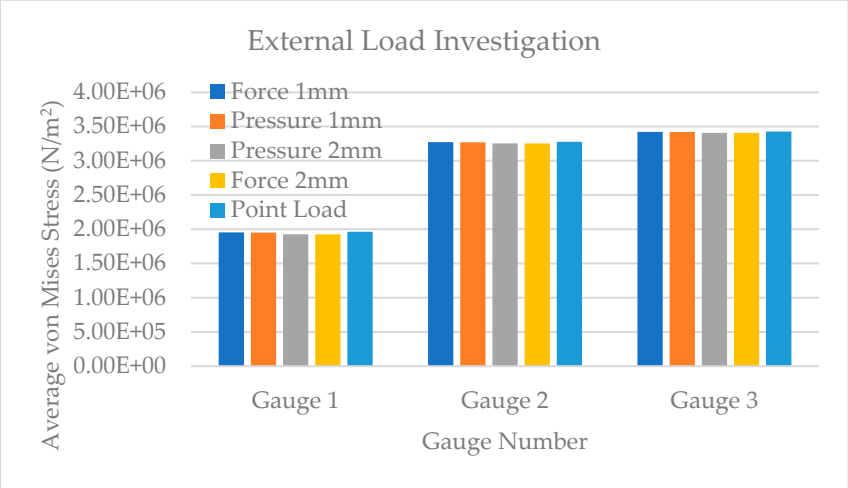

Figure 10. External load investigation

This also proved that when physically applying the load, the shape of the contact of the load applicator (size of the ball bearing etc.) would not significantly impact the stress at the locations of the strain gauges.

3.3. Maximum Load

A robust knee transducer should be able to withstand 450 N. This is based on the criteria used by other investigators identified during literature search.

Using Aluminum, it was necessary to establish a factor of safety (FOS). Using the boundary conditions established previously, the FOS for the system was explored. The minimum acceptable FOS for this application was set to 1.5. The total load was applied to both the medial and lateral compartments in the center of each compartment and as near as possible to the edge as seen in (Figure 11).

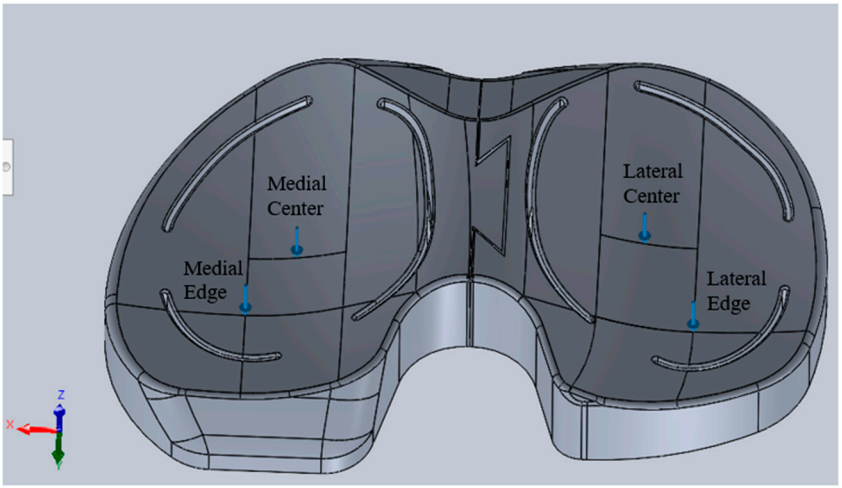

Figure 11. Locations of applied loads for maximum load investigation.

The results indicated that using aluminum alloy results in low factor of safety close to the edge of the sensing area where large overhang exists between the adjacent tabs. Using alloys of Titanium (Yield Strength=500 MPa) proved to be a much more suitable material for this transducer. It may also be necessary to run a similar FOS test but against vertical deflection of the overhang areas of the sensor outside the straight sided triangles formed by linking the 3 tabs using straight line. Using Titanium or a high specification steel alloy will ensure that 450 N could be applied over the entire surface of each compartment.

 doi:10.20944/preprints202404.1464.v1

Table 2. FOS with 450 N Applied to the Surface.

	Medial		Lateral	
	Center	**Edge**	**Center**	**Edge**
Aluminium Alloy	2.96	1.78	1.59	0.75
Titanium	-	-	-	1.60

3.4. Stress Raises

The next exercise was to create stress raisers to improve signal to noise ratios. For that reason, slits were created to magnify the sensitivity of the device and to reduce the possibility of any mechanical crosstalk. To develop the AI to give a unique solution an inverse problem-solving approach was adapted. The inverse problem approach was in the form of, an ANN used to determine the magnitude and location of the unique external load that generated those strains or voltages, in this case. Using Solidworks, Finite Element Analysis (FEA) and superposition to train the ANN it was possible to find the instantaneous values of strains obtained from the 3 strain gauges to predict the exact location and magnitude of the load that caused them in real time. By raising the stresses in the tabs where the strain gauges were placed a good signal to noise ratio can be ensured. To prove this was the case, 450 N was applied to each compartment like the previous section. However, in this case, the von Mises stress was recorded from 6 different equidistant points leading up to the centre of the strain gauge. Figure 12 depicts how the 6 points are arranged linearly from the centre of the sensor towards the centre of the strain gauge in 0.5 mm increments.

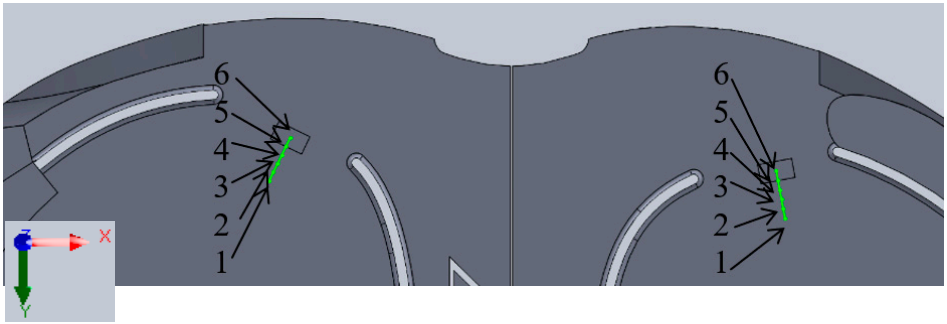

Figure 12. Locations of stress raises towards strain gauges.

Figure 13 depicted how the stress increased along the path to the strain gauge. This proved the impact of adding the slits for the sensitivity of results, where the stress distribution can be seen in Figure 14.

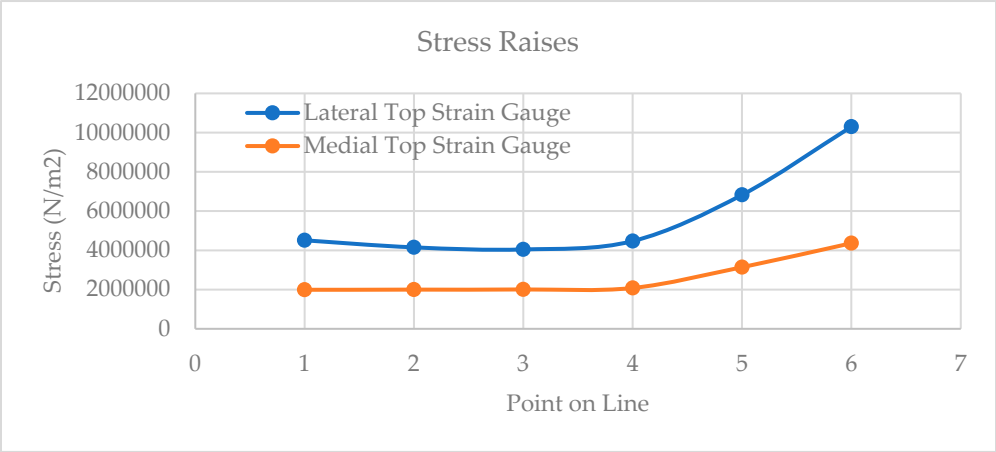

Figure 13. Stress raises results.

 doi:10.20944/preprints202404.1464.v1

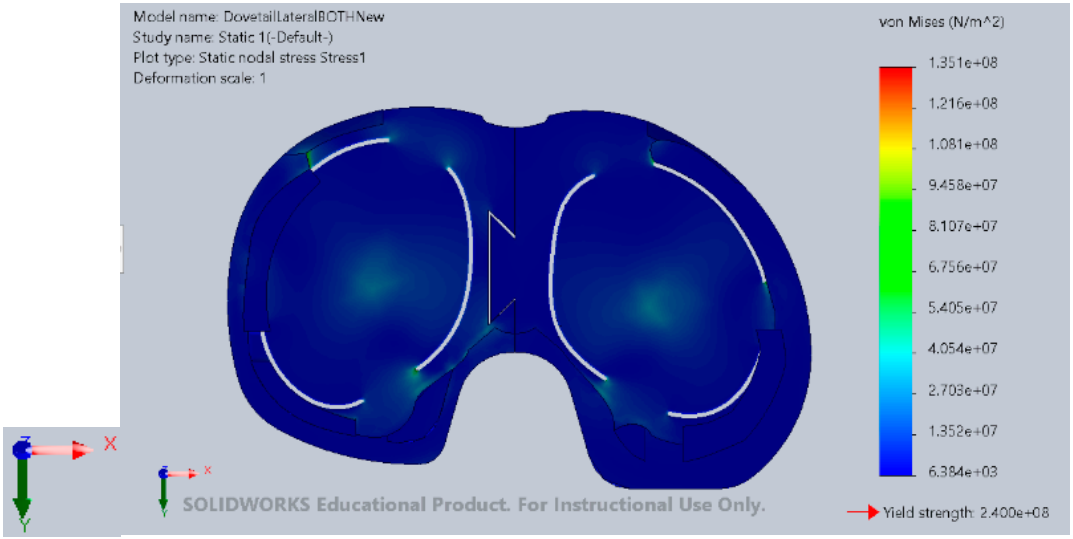

Figure 14. Stress distributions (stress raises at tabs).

3.5. Load Sharing

The goal of this device was to measure the load in each compartment to ensure the two were balanced. For the results to be accurate there should not be any load sharing between compartments. The same boundary conditions remained, including the interaction between the two parts to be contacted. To ensure the load was isolated to each compartment, a very high point load (700 N) was applied to the medial compartment, while the stress at each gauge was recorded from the lateral compartment, then the opposite was done.

Table 3 noted that the average von mises stress recorded from the strain gauges were close to zero when the load was applied to the opposite compartment indicating that the load sharing between compartments was minimal. The results could be visualised in Figure 15a,b.

Table 3. Average Von Mises stress on the strain gauge from the opposite compartment of applied load.

	Medial Compartment			Lateral Compartment		
	Gauge 1	**Gauge 2**	**Gauge 3**	**Gauge 1**	**Gauge 2**	**Gauge 3**
Von Mises Stress (N/m²)	2.65E-03	1.72E-03	1.87E-03	1.53E-03	1.24E-02	1.66E-02

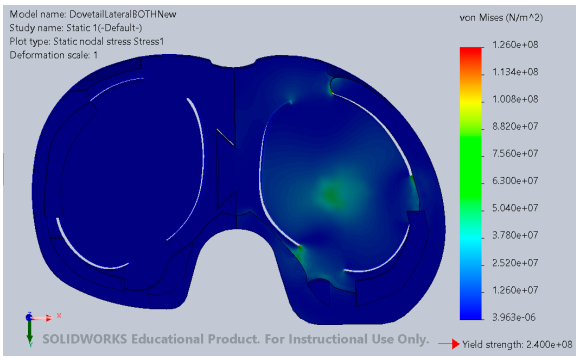

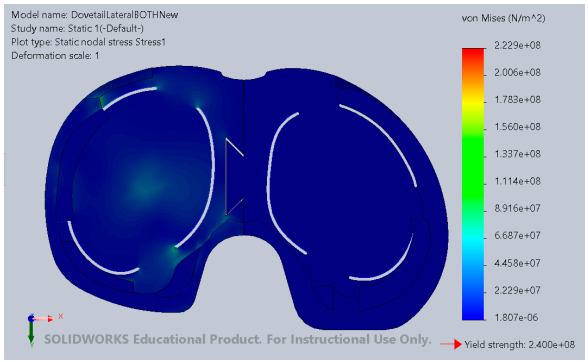

 doi:10.20944/preprints202404.1464.v1

(**a**) (**b**)

Figure 15. Stress from 700 N point load **a)** Load applied to medial compartment **b)** Load applied to lateral component.

4. Fabrication

The fabrication of the tibial sensor involved creating the physical design based on the drawings, the electronics of the sensor, and the artificial intelligence to create the link between the electronics and loads.

4.1. Physical Fabrication

Due to the unknown stress concentrations that arise when an object is 3D printed, it was determined that CNC aluminum alloy would be ideal for prototyping (Figure 16). Limitations of machining prevented the dovetail and size of slits from matching the drawings; however future iterations would overcome this. Moreover, an aluminum alloy was chosen for a first prototype since is was cheaper and easier to fabricate and because stress is material independent the results can be easily translated to titanium when the sensor is further developed.

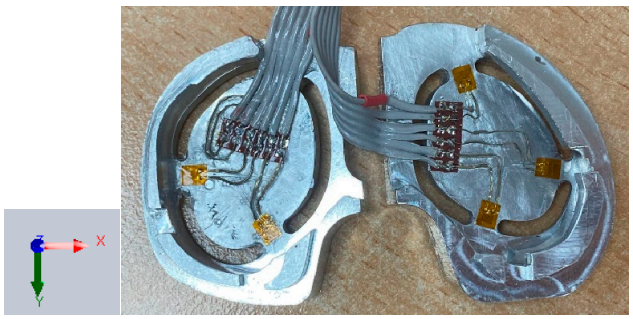

Figure 16. First prototype of tibial sensor.

4.2. Electronics

Based on the literature surrounding knee force sensors a few were considered for this application: metal-bonded strain gauges, piezoresistive strain gauges, and piezoelectric. Strain gauges are small, flexible, and can be attached to the surfaces of the sensor where deflection causes the strain gauges to change resistance. Nolten et al. used piezoresistive pressure sensors for their intraoperative load sensor for knee replacements; however, this sensor had a limit of 100 N (10.20 kg) which was unsuitable [17]. The limited sensing range was not an inherent characteristic of the piezoresistive gauges; however, due to the nonlinearity with strain, it was thought that the AI would have a more difficult time converging with this data. Another research used piezoelectric sensors, but again the sensing region was below 50 N (9.81 kg) [25]. Moreover, piezoelectric sensors were typically used for measuring dynamic pressure. Consequently, to have a good tradeoff between sensing region, sensitivity, robustness, and cost metal-bonded strain gauges were chosen. Other research measuring intraoperative load in the knee also utilized metal- bonded strain gauges [12,19,20,27] .

For this sensor three 350 Ohm (SGT-1/350-TY11) precision metal-bonded strain gauges were used as the sensors in each compartment plus the same amount for temperature compensation. This

Preprints.org (www.preprints.org) | NOT PEER-REVIEWED | Posted: 23 April 2024 doi:10.20944/preprints202404.1464.v1

totaled to 12 gauges for one sensor. The use of three was necessary in providing the AI with enough data to predict accurately and precisely based on the size and shape of the tibial insert surface.

A Wheatstone bridge was used for this application as it can measure small changes in resistance in electrical circuits from the load applied to the surface. When the load was applied to the device there was a change in resistance of the gauges which caused a change in voltage where the Wheatstone bridge became unbalanced. The half bridge configuration of the Wheatstone bridge was utilized since there was need to compensate for change in temperature experienced by the strain gauges.

One bridge consists of four resistors arranged in a bridge configuration with a voltage source (5 V) applied. In this application two resistors were replaced with two strain gauges (350 Ω), one that was active and the other that was passive for temperature compensation. The other two resistors were 470 Ω and since they were equal, balanced. When referring to Figure 17 the unloaded sensor is balanced and the relationship between the resistances is:

$$\frac{R1}{R3} = \frac{R2}{R4} \tag{1}$$

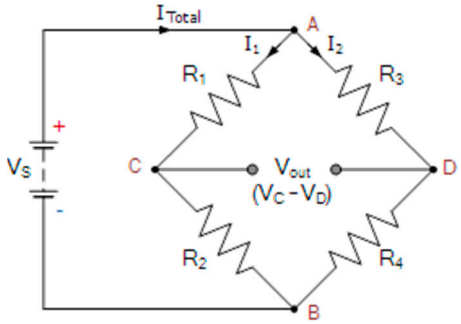

Figure 17. Wheatstone bridge.

The Wheatstone bridge configuration was repeated three times for each side. To increase the amount of input data from the sensor there was an option to increase the amount of Wheatstone bridges to 4; however, this also would increase the cost and complexity of the sensor and without any indication that a fourth would be needed.

The output of the Wheatstone bridge was amplified (Load Cell Amplifier (HX711 by SparkFun) and connected to a microcontroller (Teensy 4.1 Microcontroller) expressed by Figure 18. The printed circuit board (PCB) to integrate the Wheatstone bridge, the amplifier, and the microcontroller can be seen in Figure 19.

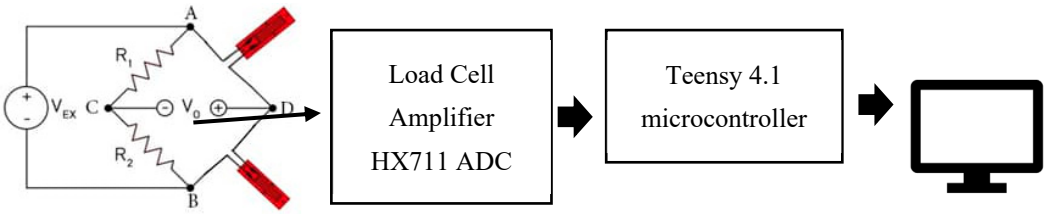

Figure 18. Electronics configuration .

 doi:10.20944/preprints202404.1464.v1

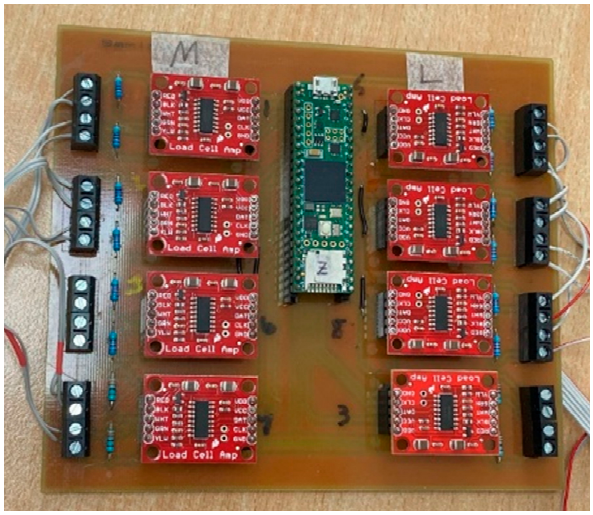

Figure 19. Printed circuit board.

Artificial Intelligence

The goal of this sensor was to be able to sense contact loads all over the surface of the sensor. With the absence of any closed form relationship between force, position, and strain on the tabs the use of artificial intelligence (AI) was employed. With AI the sensing area increased by over 150% for each compartment as seen in Figure 20.

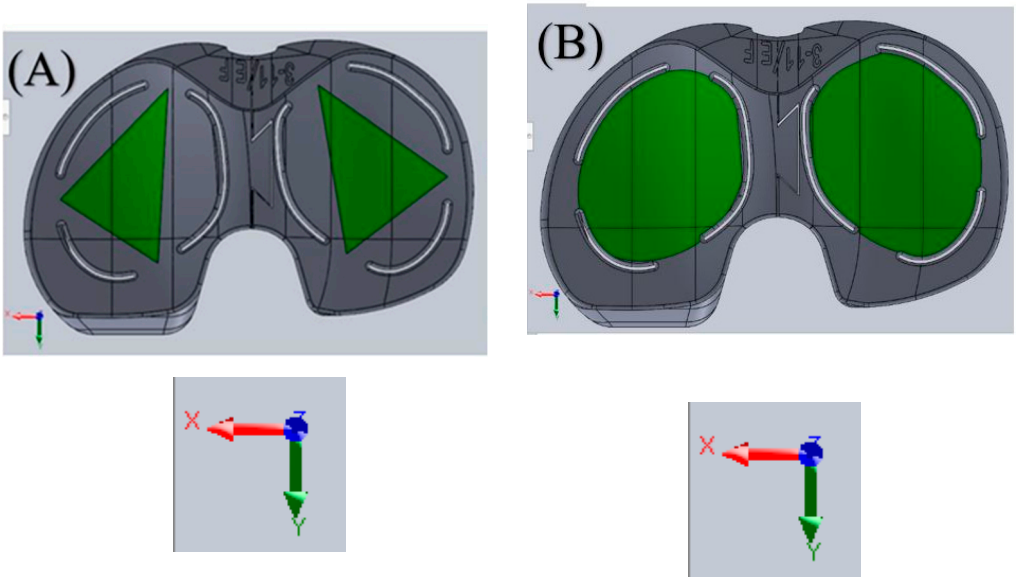

(**a**) (**b**)

Figure 20. Sensing area **a)** Without AI **b)** With AI.

Specifically, an artificial neural network (ANN) was chosen since it was best suited for this type of prediction problem as described by Table 4 where the three strain values were used as a function of the load and location.

Table 4. Types of AI.

Type	Use	Advantage	Disadvantage
Machine Learning (ML)	Classification Problems	Can identify trends or patterns	Requires manual feature extraction

 doi:10.20944/preprints202404.1464.v1

Artificial Neural Network (ANN)	Pattern classification, prediction, and control optimization	Good generalization and success with nonlinear data	Proper structure requires trial and error
Convolution Neural Network (CNN)	Image processing and object detection	Efficient image processing	High computational requirements
Recurrent Neural Networks (RNN)	Image captioning, time-series analysis, and handwriting recognition	Can process any length of input	Training can be difficult

Data was collected to train the network by creating a cartesian coordinate system on the surface of the sensor where a range of loads were applied to every location, and the output of the circuit (millivolts) was recorded. Following the collection of the data, further loads were extrapolated at each point, pre-processed, and then network optimization begun. This included optimizing different parameters and hyperparameters of the network until convergence. After the network was trained and optimized, it was used in real time to predict the load and its location over the surface of the sensor.

Moreover, after the FEA model was validated with the practical model, data could be collected for training and optimization of the network. This would reduce the time and the errors associated with manual collection of training data. This novel use of FEA could increase the scalability of the sensors for mass production and fast training of individual designs.

Furthermore, the physical training procedure for the final prototype would benefit from automation via robotics which would increase the repeatability and the consistency of physically collected training data. This would increase the robustness of the AI and increase its ability for generalisation and reaching of the global minimum. Further details on the network used for this sensor can be found in [27,28].

4.3. Validation

The validation of the electronics compared to the FEA was investigated next. First, to validate the results from the electronics the strain was collected from a strain indicator (Figure 21). Following this, the results were validated using the strain produced by FEA.

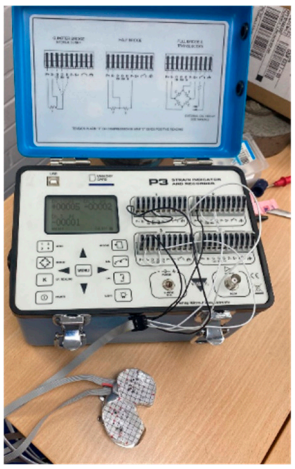

Figure 21. Sensor connected to strain indicator.

A point was chosen from the surface of the lateral compartment of the sensor (2,2). Then, three points loads were applied to the surface: 5 kg, 15 kg, and 25 kg. The results from both the sensor's PCB and the strain indicator were recorded. Once normalised, the results of the three gauges were nearly identical between the strain values and the amplified voltage values as seen in Figure 22.

 doi:10.20944/preprints202404.1464.v1

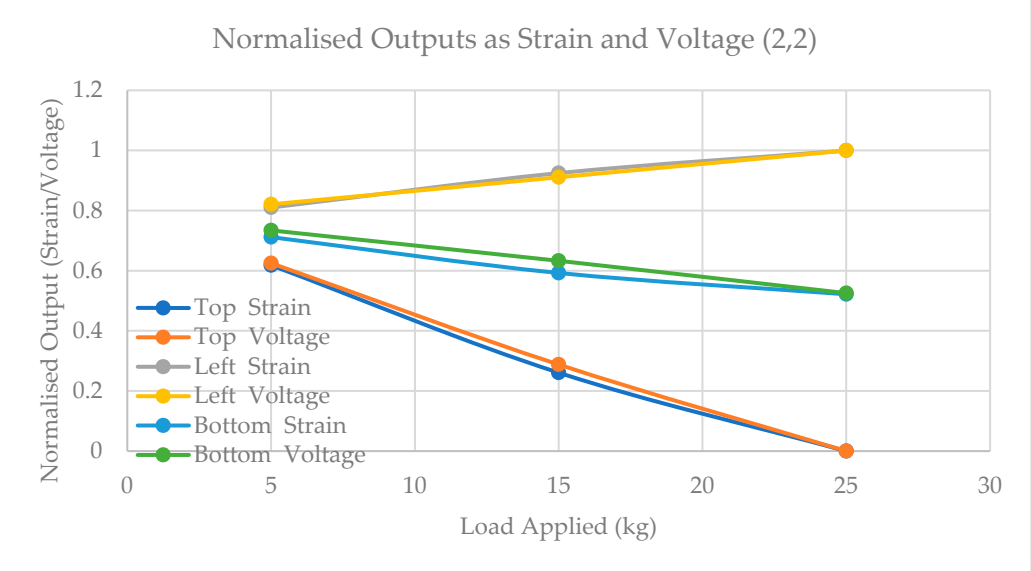

Figure 22. Comparison of sensor outputs as strain (strain indicator) and voltage (self-made PCB) from point (2,2).

Next, the CAD drawing was altered to mimic the fabricated sensor, including the Cartesian grid system (Figure 23).

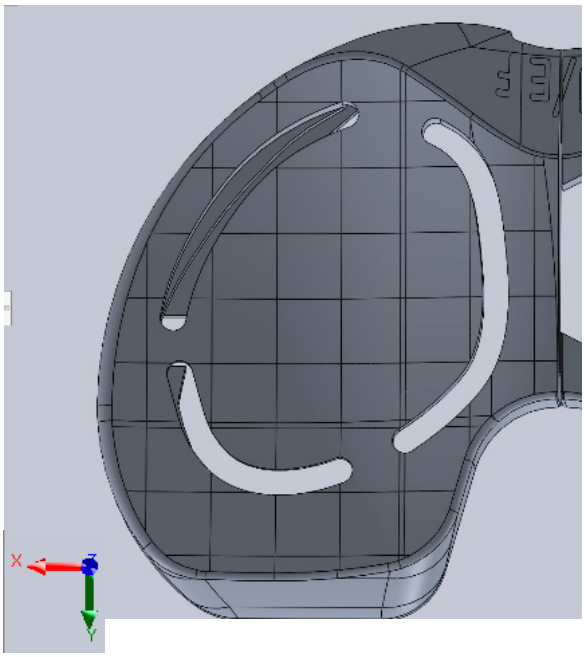

Figure 23. Model of sensor based on fabricated part.

The principal strains were compared with the strains collected from the sensors at the same points and the considering discrepancies between the model and the physical sensor were similar, indicating that the results from the FEA were valid.

Preprints.org (www.preprints.org) | NOT PEER-REVIEWED | Posted: 23 April 2024 doi:10.20944/preprints202404.1464.v1

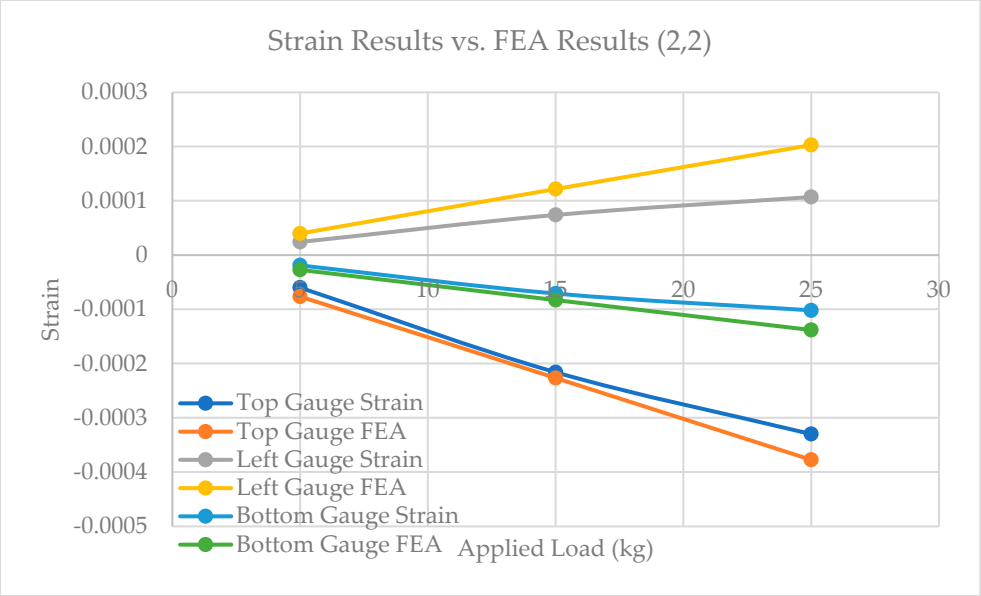

Figure 24. Validated FEA of each gauge.

The validation of the FEA provided a tool for network training for the artificial intelligence where FEA can be used to collect strain data. The results can be converted back to the voltage once the network is trained to be able to use the network in real time.

5. Conclusion

In conclusion, the literature surrounding intraoperative sensors has informed the design of this sensor. The design allowed loads of up to 450 N to be applied while increasing the sensitivity, reducing mechanical crosstalk, and minimising load sharing. Additionally, the curved surface design remained to fit with the femur as well as the adjustable rings for varying the tension in the knee. In total, the design of this sensor incorporated all the elements of an accurate and robust tool for intraoperative use which were determined by literature.

Furthermore, the use of AI allowed for sensing over the whole surface while maintaining high accuracy and precision for both the prediction of the load and the location. This would be the first sensor able to bridge this gap in the market where a sensor fulfilling all these points does not currently exist, as far as the authors know.

Additionally, FEA proved to be a valuable to for design optimisation, material selection, and for AI optimisation by allowing for the collection of training data and investigation of the impact of physically collected training data. Additionally, since the FEA was validated, the model can be used to train the network and optimise parameters.

The limitations of this design include ability to machine fine details; however, due to this sensor being the first prototype further details will be added along with the use of a stronger more expensive material. This research was aimed to demonstrate a concept which integrates various design elements outlined in literature to cover a gap in the market vital to the success of TKRs. Once commercialised, limitations previously mentioned will be easily overcome.

The goal of this device is to restore function in the knee by ensuring proper tension is set during TKRs. Providing surgeons with this tool would increase patient outcomes and reduce costs for the insurance companies, stakeholders, biomedical companies, and regulatory bodies like the NHS. Patients could also recover from surgery faster and maintain and wider ROM postoperatively. Moreover, following a sensor balanced knee replacement, patients should have proper gait symmetry due to the proper kinematics set by the load balancing of the compartments.

Author Contributions: S.A. was responsible for the first draft and methodology. S.N. was responsible for reviewing, methodology, conceptualization, and funding acquisition. A.H. was responsible for reviewing and funding acquisition.

Funding: This research was completed as part of a match funded PhD by Zimmer Biomet and Bournemouth University.

Conflicts of Interest: The authors declare no conflicts of interest.

References

1. L. Blankevoort, R. Huiskes, and A. De Lange, 'Recruitment of knee joint ligaments', Journal of Biomechanical Engineering : Transactions of the ASME, vol. 113, no. 1, pp. 94–103, 1991, doi: 10.1115/1.2894090.
2. C. Halewood and A. A. Amis, 'Clinically relevant biomechanics of the knee capsule and ligaments', Knee Surgery, Sports Traumatology, Arthroscopy, vol. 23, no. 10, pp. 2789–2796, Oct. 2015, doi: 10.1007/S00167-015-3594-8/TABLES/2.
3. I. Sanz-Pena, G.E. Zapata, M.A. Verstraete, P.A. Meere, and P. S. Walker, 'Relationship Between Ligament Forces and Contact Forces in Balancing at Total Knee Surgery.', J Arthroplasty, vol. 34, no. 6, pp. 1261–1266, Jun. 2019, doi: 10.1016/j.arth.2019.02.016.
4. D. Crottet, T. Maeder, D. Fritschy, H. Bleuler, L.P. Nolte, and I. P. Pappas, 'Development of a force amplitude- and location-sensing device designed to improve the ligament balancing procedure in TKA.', IEEE Trans Biomed Eng, vol. 52, no. 9, pp. 1609–1611, Sep. 2005, doi: 10.1109/TBME.2005.851504.
5. C. Batailler, J. Swan, E.S. Marinier, E. Servien, and S. Lustig, 'Current role of intraoperative sensing technology in total knee arthroplasty', Arch Orthop Trauma Surg, vol. 141, no. 12, pp. 2255–2265, 2021, doi: 10.1007/s00402-021-04130-5.
6. S. J. MacDessi, J.A. Wood, A. Diwan, and I. A. Harris, "Intraoperative pressure sensors improve soft-tissue balance but not clinical outcomes in total knee arthroplasty: a multicentre randomized controlled trial.," *Bone Joint J*, vol. 104-B, no. 5, pp. 604–612, May 2022, doi: 10.1302/0301-620X.104B5.BJJ-2021-1299.R2.
7. S. Ghirardelli, A. Bala, G. Peretti, G. Antonini, and P. F. Indelli, 'Intraoperative Sensing Technology to Achieve Balance in Primary Total Knee Arthroplasty: A Review of the Literature', JBJS Rev, vol. 7, no. 10, pp. 1–6, 2019, doi: 10.2106/JBJS.RVW.19.00008.
8. P. F. Sharkey, P.M. Lichstein, C. Shen, A.T. Tokarski, and J. Parvizi, 'Why are total knee arthroplasties failing today—has anything changed after 10 years?', J Arthroplasty, vol. 29, no. 9, pp. 1774–1778, 2014.
9. K. Gustke (a), G.J. Golladay, M.W. Roche, L.C. Elson, and C. R. Anderson, 'Primary TKA Patients with Quantifiably Balanced Soft-Tissue Achieve Significant Clinical Gains Sooner than Unbalanced Patients.', Adv Orthop, vol. 2014, p. 628695, 2014, doi: 10.1155/2014/628695.
10. A. T. Livermore, J.A. Erickson, B. Blackburn, and C. L. Peters, 'Does the sequential addition of accelerometer-based navigation and sensor-guided ligament balancing improve outcomes in TKA?', Bone Joint J, vol. 102-B, no. 6_Supple_A, pp. 24–30, May 2020, doi: 10.1302/0301-620X.102B6.BJJ-2019-1634.R1.
11. J. D. Roth, S.M. Howell, and M. L. Hull, 'An Improved Tibial Force Sensor to Compute Contact Forces and Contact Locations In Vitro After Total Knee Arthroplasty.', J Biomech Eng, vol. 139, no. 4, Apr. 2017, doi: 10.1115/1.4035471.
12. K. R. Kaufman, N. Kovacevic, S.E. Irby, and C. W. Colwell, "Instrumented implant for measuring tibiofemoral forces," *J Biomech*, vol. 29, no. 5, pp. 667–671, 1996, doi: 10.1016/0021-9290(95)00124-7.
13. Skrinskas, T.V., D.G. Viskontas, L. Ferreira, D.G. Chess, and J. A. Johnson. 'Application of an intra-operative load measuring system for knee replacement surgery.', Medical Image Computing and Computer-Assisted Intervention-MICCAI 2003: 6th International Conference, Montréal, Canada, November 15-18, 2003. Proceedings 6, pp. 246-253. Springer Berlin Heidelberg, 2003.R. C. Wasielewski, D.D. Galat, and R. D. Komistek, "An intraoperative pressure-measuring device used in total knee arthroplasties and its kinematics correlations," *Clin Orthop Relat Res*, vol. 427, no. 427, pp. 171–178, 2004, doi: 10.1097/01.blo.0000145555.34318.46.
14. D. Crottet, T. Maeder, D. Fritschy, H. Bleuler, L.P. Nolte, and I. P. Pappas, "Development of a force amplitude- and location-sensing device designed to improve the ligament balancing procedure in TKA.," *IEEE Trans Biomed Eng*, vol. 52, no. 9, pp. 1609–1611, Sep. 2005, doi: 10.1109/TBME.2005.851504.
15. B. Jeffcote, R. Nicholls, A. Schirm, and M. S. Kuster, "The variation in medial and lateral collateral ligament strain and tibiofemoral forces following changes in the flexion and extension gaps in total knee replacement," *J Bone Joint Surg Br*, vol. 89-B, no. 11, pp. 1528–1533, 2007, doi: 10.1302/0301-620X.89B11.18834.
16. U. Nolten, F. Schmidt, F.P. Firmbach, K. Radermacher, and W. Mokwa, "Sensor integrated tibial inlay for soft-tissue balancing," *Procedia Chem*, vol. 1, no. 1, pp. 1251–1254, 2009, doi: 10.1016/j.proche.2009.07.312.
17. A. Anastasiadis, E. Magnissalis, and A. Tsakonas, "A novel intraoperative sensor for soft tissue balancing in total knee arthroplasty," *J Med Eng Technol*, vol. 34, no. 7–8, pp. 448–454, 2010, doi: 10.3109/03091902.2010.517898.

18. W. Hasenkamp *et al.*, "Design and test of a MEMS strain-sensing device for monitoring artificial knee implants," *Biomed Microdevices*, vol. 15, no. 5, pp. 831–839, 2013, doi: 10.1007/s10544-013-9770-z.
19. D. Forchelet *et al.*, "Enclosed electronic system for force measurements in knee implants," *Sensors (Switzerland)*, vol. 14, no. 8, pp. 15009–15021, 2014, doi: 10.3390/s140815009.
20. M. A. Verstraete, P.A. Meere, G. Salvadore, J. Victor, and P. S. Walker, "Contact forces in the tibiofemoral joint from soft tissue tensions: Implications to soft tissue balancing in total knee arthroplasty," *J Biomech*, vol. 58, pp. 195–202, Jun. 2017, doi: 10.1016/J.JBIOMECH.2017.05.008.
21. H. Jiang, S. Xiang, Y. Guo, and Z. Wang, "A wireless visualized sensing system with prosthesis pose reconstruction for total knee arthroplasty," *Sensors (Switzerland)*, vol. 19, no. 13, 2019, doi: 10.3390/s19132909.
22. M. Safaei, S. Dupre, E. Hoummadi, and S. R. Anton, "Design, analysis, and fabrication of a piezoelectric force tray for total knee replacements," *J Intell Mater Syst Struct*, vol. 30, no. 20, pp. 3163–3176, 2019, doi: 10.1177/1045389X19880003.
23. M. Jain, N.A. Hossain, S. Towfighian, R. Willing, M. Stanacevic, and E. Salman, "Self-Powered Load Sensing Circuitry for Total Knee Replacement," *IEEE Sens J*, vol. 21, no. 20, pp. 22967–22975, 2021, doi: 10.1109/JSEN.2021.3110241.
24. F.-X. Wang *et al.*, "Novel Force Measurement System for Soft Tissue Balance in Total Knee Arthroplasty Based on Flexible Pressure Sensor Arrays," *Advanced Intelligent Systems*, vol. 4, no. 4, p. 2100156, 2022, doi: 10.1002/aisy.202100156.
25. S. Kuriyama, K. Nishitani, S. Nakamura, and S. Matsuda, "An electronic force sensor accurately detects increased but not decreased soft tissue tension in total knee arthroplasty," *Knee*, vol. 42, pp. 210–219, 2023, doi: 10.1016/j.knee.2023.03.020.
26. T. V Skrinskas, D.G. Viskontas, L. Ferreira, D.G. Chess, and J. A. Johnson, 'Application of an Intra-operative Load Measuring', pp. 246–253, 2003.
27. S. Al-Nasser, S. Noroozi, A. Harvey, N. Aslani, and R. Haratian, "Exploring the Performance of an Artificial Intelligence-Based Load Sensor for Total Knee Replacements," Sensors, vol. 24, no. 2, 2024, doi: 10.3390/s24020585.
28. S. Al-Nasser, S. Noroozi, R. Haratian, N. Aslani, and A. Harvey, "Load Prediction using an Intraoperative Joint Sensor and Artificial Neural Network," 19th International Conference on Condition Monitoring and Asset Management, CM 2023, p. 2024, 2023, doi: 10.1784/cm2023.4f2.